ACADEMIA ROMÂNĂ
Revue Roumaine de Chimie
http://web.icf.ro/rrch/

Rev. Roum. Chim.,
2017, *62*(12), 923-931

EVALUATION OF CORROSION BEHAVIOUR AND SURFACE CHARACTERIZATION FOR SOME BIOMEDICAL MATERIALS

Florina BRANZOI,[a*] Mihai IORDOC[b] and Viorel BRANZOI[c]

[a] Institute of Physical Chemistry of Roumanian Academy, Spl Independentei 202, 060021, Bucharest, Roumania
[b] National Institute for Research and Development in Electrical Engineering ICPE-CA, 313 Splaiul Unirii, District 3, 030138, Bucharest, Roumania
[c] University Politehnica of Bucharest, Faculty of Applied Chemistry and Materials Science, 1-7 Gheorghe Polizu St., Sector 1, 011061, Bucharest, Roumania

Received December 22, 2016

The aim of this work is to study the influence of Nb and Ta amount on the growth of zirconia ceramic films in alkaline electrolyte on ZrNbTa ternary biomedical alloys by Plasma Electrolytic Oxidation technique (PEO) and to demonstrate the surface properties improvement after this process. Samples of Zr2.5Nb3Ta (medium alloyed ZrNbTa alloy) and Zr10Nb12Ta (high alloyed ZrNbTa alloy) ternary alloys were obtained through a cycling melting process in an induction furnace and were developed to be used in orthopedic surgery for total hip and total knee replacement. The surface characterization and corrosion behavior of as-cast and oxidized medium and high alloyed ZrNbTa alloys were investigated in fetal bovine serum (FBS) at 37^0C and atmospheric pressure without agitation, using Electrochemical Impedance Spectroscopy (EIS) and Potentiodynamic Polarization as electrochemical techniques. As surface characterization techniques we used SEM, X Ray Diffraction (XRD) and Vickers micro-hardness and interferometry measurements. Ion release phenomena were investigated using Inductive Coupling Plasma – Mass Spectrometry technique (ICP MS). XRD analysis was used to identify the chemical composition of the outer oxide layer and pointed out the formation of two zirconium oxides consist of a black non-stoichiometric zirconium oxide layer and a small amount of white stoichiometric zirconium oxide which has poor quality. Laboratory studies have demonstrated that the increase of the Nb and Ta amount from alloys led to the improving of surface micro-hardness and electrochemical behavior of these metallic biomaterials in Fetal Bovine Serum. During the plasma electrolytic oxidation process, a zirconium oxide layer of about 50 microns is formed on the alloy surface, which improves corrosion resistance and surface micro-hardness.

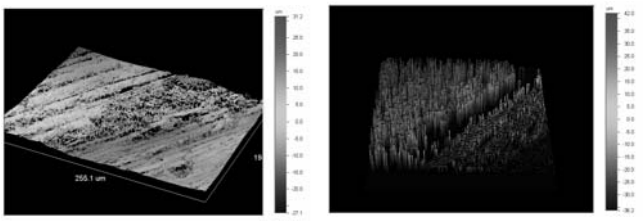

INTRODUCTION

Plasma electrolytic oxidation (PEO), known as micro-arc oxidation technique[1,2] is a novel electro-chemical surface treatment process for generating oxide coatings on valuable metals such as Al, Mg, Ti, Zr and their alloys, which is characterized by a high temperature of 10^3 to 10^4 K and a high local pressure of 10^2 to 10^3 MPa in the discharge channels.[3,4] Earlier research showed that the coatings offered an attractive combination of wear resistance, corrosion resistance, mechanical strength, interfacial adhesion, chemical stability, high temperature shock resistance, etc.[5-10] During the oxidation processes, zirconium and its alloys form surface films consisting of a mixture of two oxides and gas-saturated layers, *i.e.*, interstitial solid solutions of oxygen atoms in the zirconium matrix. According to the Zr – O_2 state diagram, there is a single ZrO_{2-x} oxide in which the concentration of oxygen can vary with temperature. The black nonstoichiometric

* Corresponding author: fbrinzoi@icf.ro

zirconium oxide possesses protective properties. At the same time, the white stoichiometric oxide is porous and does not protect the alloy.[11] Moreover, dense protective films of zirconium oxide formed by plasma electrolytic oxidation may significantly increase the corrosion resistance of the zirconium alloy.[12] There is current interest in the biological chemistry of Zr. Zirconium metal is widely used in artificial joints for limbs, and in metal-on-metal and alternative material combinations for hip replacements.[13-15] Zirconium oxide is a bio-inert material that exhibits high mechanical strength, excellent corrosion resistance and good biocompatibility.[16] It is frequently used in manufacture of hip head prostheses.[17,18] The biocompatibility and osseointegration of zirconium oxide has been largely demonstrated in vitro and in vivo. Many authors observed that zirconium oxide has no cytotoxic effects when fibroblasts were co-cultured with it.[19] Additional studies reported that zirconium oxide does not generate mutations of the cellular genome.[20] No adverse responses were reported following the insertion of zirconium oxide into bone or muscle in "*in vivo*" models.[18] Zirconium oxide creates less phlogistic reaction in tissue than other restorative materials such as titanium.[21] This observation was confirmed by a study comparing soft tissue around zirconia and titanium healing caps: inflammatory infiltrate, micro vessel density, and vascular endothelial growth factor expression were higher around the titanium caps than around the zirconia ones.[18,22]

In this article, we studied the influence of Nb and Ta amount on the growth of zirconia ceramic films in alkaline electrolyte on ZrNbTa ternary biomedical alloys by Plasma Electrolytic Oxidation technique (PEO) and we demonstrated the surface properties improvement after this process. The surface characterization and corrosion behavior of as-cast and oxidized medium and high alloyed ZrNbTa alloys were investigated in fetal bovine serum (FBS) at 37°C and atmospheric pressure without agitation, using Electrochemical Impedance Spectroscopy (EIS) and Potentiodynamic Polarization as electrochemical techniques. As surface characterization techniques we used SEM, X Ray Diffraction (XRD) and Vickers micro-hardness and interferometry measurements.

EXPERIMENTAL

Prior to PEO process and electrochemical experiments, the ZrNbTa samples were polished with SiC emery paper down to #4000. After polishing, the samples were degreased in acetone ultrasonic bath for 30 min and then washed with Millipore water and then immersed in the electrolyte for PEO treatment. The electrolysis environment was an aqueous electrolyte containing NaOH, Na_2SiO_3 and NaCl at concentrations of 2 g/L, 8 g/L and 0.5 g/L respectively. A PEO coating unit designed and built by the authors has been employed in the present study, which mainly consists of a power supply unit, a bath container and a cooling system. The metallic samples immersed in the electrolyte were used as the anode and paramagnetic stainless steel bath was used as the counter electrode. Throughout the entire range of experimentation, the temperature of the electrolyte was maintained constant at approximately 25°C and the electrolyte was mixed with a magnetic stirrer. The experiment was carried out for 10 minutes at 2500A/m^2 and voltages up to 1000V.

A VoltaLab 40 model electrochemical combine with dynamic EIS (Electrochemical Impedance Spectroscopy) connected to a computer through VoltaMaster 4 Software interface was used for the electrochemical measurements. The electrochemical behavior of as-cast and oxidized zirconium alloys was studied in a classical electrolytic cell with three electrodes. A platinum plate electrode and a saturated calomel electrode (SCE) were used as counter and reference electrode respectively. All three electrodes were placed in a cell which has been connected to a UltraThermostat type U10 with external recirculation of heating water to maintain the temperature inside the cell very close to 37 ^{0}C. The working electrode was made from as-cast Zr2.5Nb3Ta, as-cast Zr10Nb12Ta, oxidized Zr2.5Nb3Ta (Ox-Zr2.5Nb3Ta) and oxidized Zr10Nb12Ta (Ox-Zr10Nb12Ta) alloy respectively. Samples with 1 cm^2 geometric surface area were used. The working electrode potential was scanned on the potential range of -1000 mV up to +1000 mV/SCE with scan rate of 0.5 mV/sec. This scan potential range was chosen taking into account that, the potential – pH diagram given by Black[23] for generally physiological conditions showed that, the potential value of a metallic biomaterial may vary from -1.0 to +1.0 V/SCE in the human body.

Impedance measurements were performed on the frequency range between 100 kHz and 1 mHz with an AC wave of ± 5 mV (peak-to-peak) overlaid on a DC bias potential and the impedance data were obtained at a rate of 10 points per decade change in frequency.

All tests have been performed in FBS with the chemical composition given in Table 1, at 37 ^{0}C under atmospheric oxygen conditions without agitation.

The X-Ray Diffraction (XRD) measurements were performed using a Bruker-AXS X Ray Diffractometer type D8 ADVANCE device with the following characteristics: X-Ray tube with Cu anode (λ = 1.54184 Å); 40 kV / 40 mA, Ni filter k_β; Step 0.04º, measuring time on point 2 s.

The equipment employed to make determination of ultra-trace analysis is an ICP-MS made by Perkin Elmer, model ELAN DRC-e (with reaction cell gas).

Micrographs were obtained using a CARL ZEISS AURIGA Scanning Electron Microscope with OXFORD INCA ENERGY EDX module.

For the Vickers micro-hardness evaluation of the samples surface it was used a micro-hardness tester FM 700 at 2 kgf load and Wyko NT1100 system with VSI (vertical scanning interferometry) mode was used for 3D surface scanning of DLC-c-NiTi sample and DLC layer thickness measurements.

Table 1

Chemical composition of Fetal Bovine Serum

Electrolyte	Composition
Fetal Bovine Serum	Bilirubin – 2.4 mg/l; Cholesterol – 340 mg/l; Creatinine – 27.3 mg/l; Urea – 260 mg/l; Na^{+} - 142 mmol/l; Cl^{-} - 155.5 mmol/l; K^{+} - 8 mmol/l; Ca^{++} - 3 mmol/l; Mg^{++} - 1.08 mmol/l; PO_4^{3-} - 2.32 mmol/l; Fe – 1.63 mg/l; Glucose – 550 mg/l; Protein – 36 g/l; Albumine – 17 g/l; α-Globulin – 17 g/l; β- Globulin – 2 g/l; γ-Globulin – 1 g/l.

RESULTS AND DISCUSSION

The potentiodynamic polarization curves corresponding to ZrNbTa alloys are shown in Figure 1. It can be seen that all samples present similar behavior in the anode region, immediately after Tafel active region, current rises slowly reaching a limit, which translates into the formation of a stable film on the surface of the sample. After this region, there is a sudden increase in current associated with a protective film breakthrough on a narrow potential domain; the process is governed by anodic dissolution kinetics, followed by a region in which current tends to a limit value corresponding to the formation of a new film at the interface metal / electrolyte. As it can be observed than the values of the kinetic parameters showns in Table 2 point out a superior behavior from the corrosion resistance point of view for the high alloyed ZrNbTa sample (Zr10Nb12Ta).

In Figure 2 we presented the polarization curves for oxidized samples. It may be noted that the sample Ox-Zr2.5Nb3Ta in the anodic zone appear three distinct regions. The current increases very slowly in the first region which is associated with a stable film formation at the metal / electrolyte interface and the process is controlled by diffusion kinetics. The nature of passive film is protective. A second region, where the current increases sharply, is associated with the breakthrough of the passive film and the process is controlled by the dissolution kinetics. After this region, the current tends to a limit value again, which is associated with the formation of a new protective film at the interface and the kinetics is controlled by diffusion process. In the case of Ox-Zr10Nb12Ta, in the anodic zone, the sample shows only one region where the current increases slowly to a limit value.[24-30]

In this paper, the novelty is a new biomedical metal-ceramic composite with improved surface properties and higher corrosion resistance were obtained by plasma electrolytic oxidation treatment in alkaline solution. A significant improvement of corrosion resistance can be viewed, as a result of the increase of alloying elements amount and the oxidation treatment.

Nyquist diagrams corresponding to the two types of samples, respectively the ZrNbTa alloys and oxidized Ox-ZrNbTa alloys are shown in Figures 3 and 4. It can be observed that all curves shows a very well defined capacitive loops, followed by an inductive branch in the case of as-cast alloys and a diffusive branch in the case of oxidized alloys, respectively. The increase of the alloying elements amount leads tot the increase of Debye semicircles size in both cases which means a higher polarization resistance.

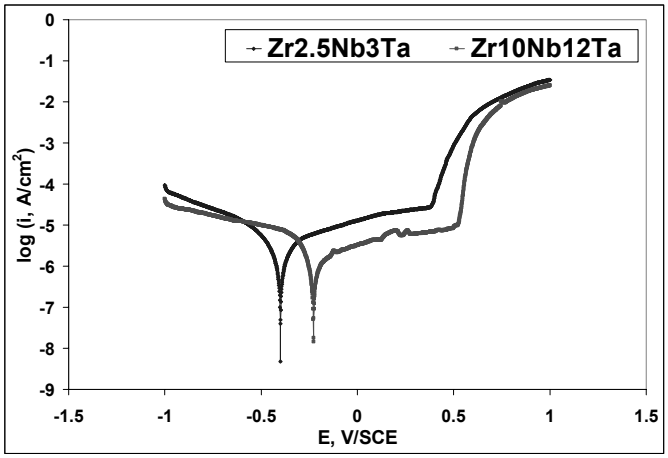

Fig. 1 – Potentiodynamic polarization curves for ZrNbTa ternary alloys.

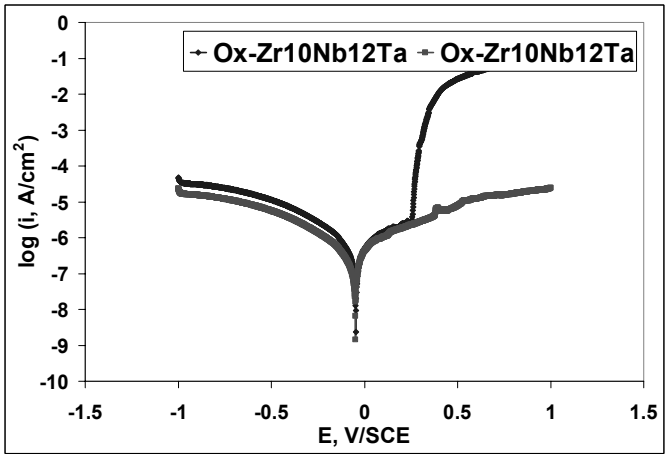

Fig. 2 – Potentiodynamic polarization curves for oxidized ZrNbTa ternary alloys.

Table 2

Corrosion kinetic parameters

No.	Electrode	E_{cor}, mV/SCE	i_{cor}, μA/cm^2	Rp, kΩcm^2	b_a, mV/dec	b_c, mV/dec	Corrosion rate, μm/year
1	Zr2.5Nb3Ta	-399.9	0.865	21.18	121.2	-106.3	9.7
2	Zr10Nb12Ta	-227.5	0.642	27.86	171.1	-87	6.79
3	Ox-Zr2.5Nb3Ta	-45.9	0.20	96.59	118.2	-127.4	3.10
4	Ox-Zr10Nb12Ta	-47.7	0.10	146.3	72.9	-127.3	1.60

Table 3

Electrochemical parameters

No.	Sample	R_{el}, Ωcm^2	R_p, kΩcm^2	C_{dl}, μF/cm^2
1	Zr2.5Nb3Ta	195	65.01	12.23
2	Zr10Nb12Ta	8.37	79.55	5.00
3	Ox-Zr2.5Nb3Ta	62	125.7	12.66
4	Ox-Zr10Nb12Ta	432.2	357.9	7.91

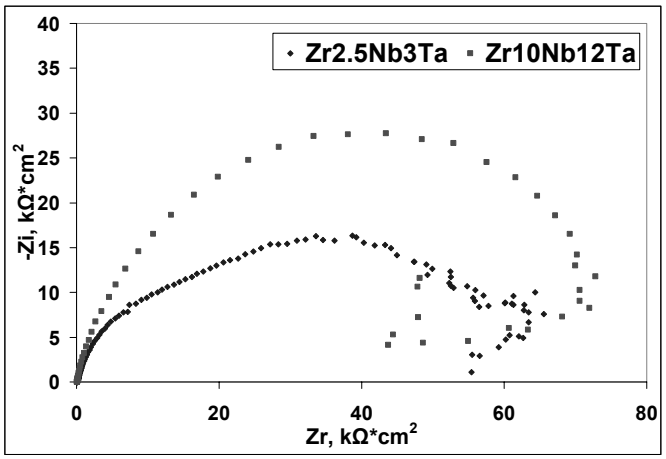

Fig. 3 – Nyquist diagrams for ZrNbTa ternary alloys.

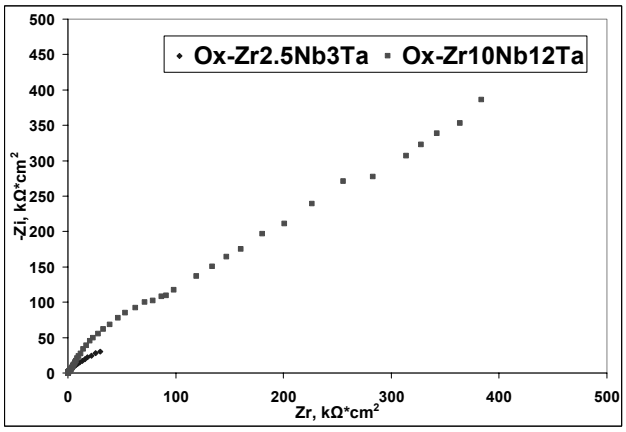

Fig. 4 – Nyquist diagrams for oxidized ZrNbTa ternary alloys.

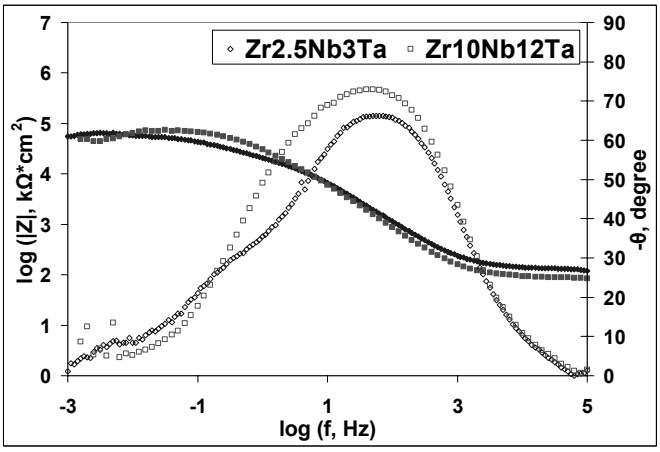

Fig. 5 – Bode diagrams for ZrNbTa ternary alloys.

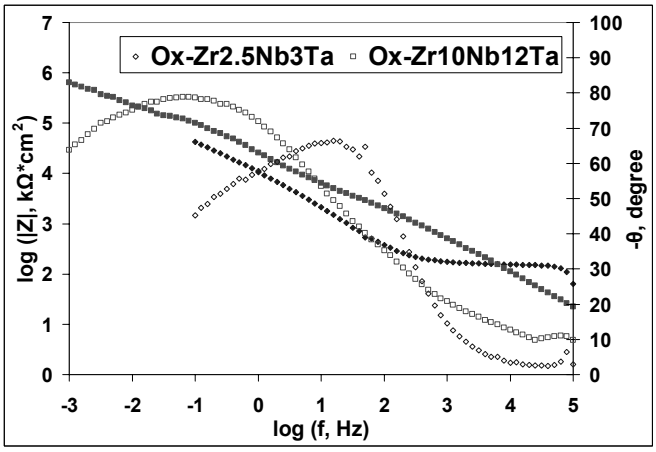

Fig. 6 – Bode diagrams for oxidized ZrNbTa ternary alloys.

From Bode diagrams (Figures 5 and 6), it can be observed that in the case of phase angle (θ) vs. log f curves of the oxidized highly alloyed sample (Ox-Zr10Nb12Ta) shows a time constant at a phase angle value of over 80^0, which points out an almost pure capacitive behavior of the film formed at the metal – electrolyte interface. In the case of medium alloyed sample, the phase angle value corresponding to time constant is lightly lower (about 70^0), fact that points out a capacitive behavior with diffusive tendencies of the interface passive film. This behavior of the films at metal –

electrolyte interface pointed out by Bode diagrams is in accordance with the observations made in the case of Nyquist diagrams.

The electrochemical parameters values shown in Table 3 reveal the superiority of the oxidized ZrNbTa alloys regarding the electrochemical behavior in fetal bovine serum electrolyte. The X-Ray patterns obtained for the two types of samples are shown in figures 7-9.

The diffraction lines translocation for Zr phase represents the consequence of Ta entering in the structure, expanding the elementary cell dimension. It can be observed that in the case of Zr10Nb12Ta sample, in which the proportion between Ta and Zr is higher than in the case of Zr2.5Nb3Ta sample, the translocation of diffraction lines is also higher. XRD can't differentiate between the Nb and Ta cubic structures. All the crystalline phases in the sample show diffraction peaks at lower diffraction angles than the ones in the files, therefore the elementary unit cell will present an increase in parameters. There are also some diffraction peaks that haven't been identified. Since they have very low intensities it is difficult to identify them.

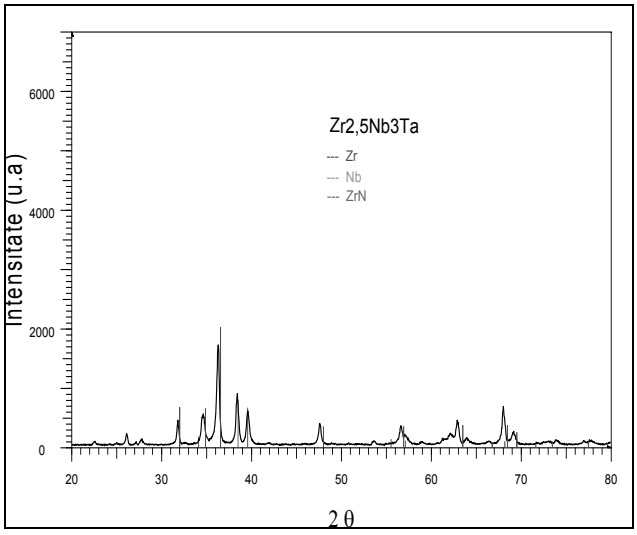

Fig. 7 – XRD pattern of Zr2.5Nb3Ta sample.

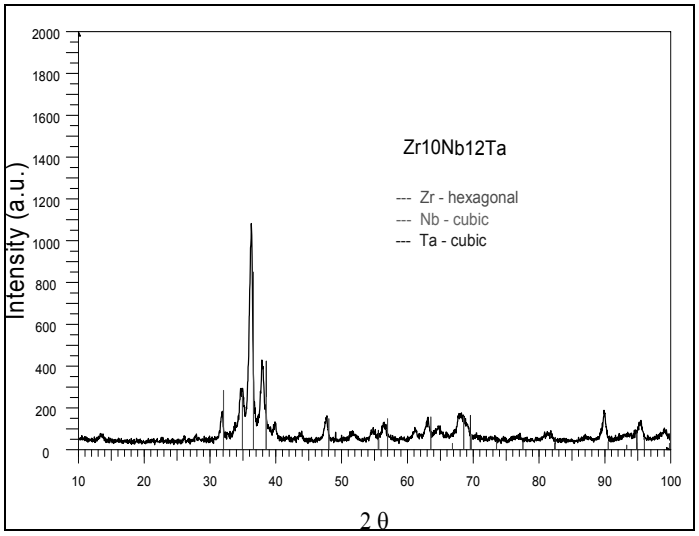

Fig. 8 – XRD pattern of Zr10Nb12Ta sample.

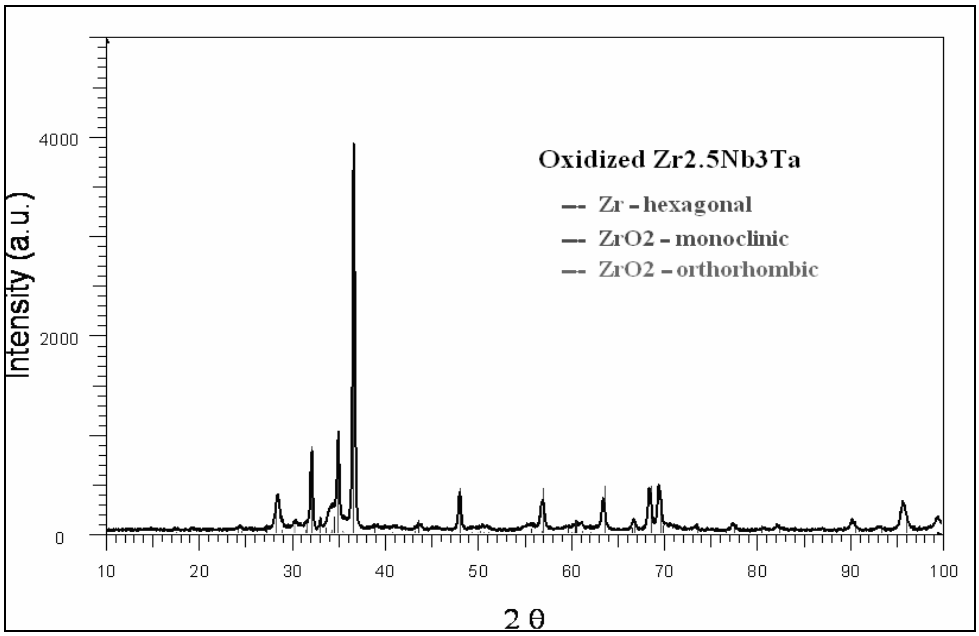

Fig. 9 – XRD pattern of Ox-Zr2.5Nb3Ta sample.

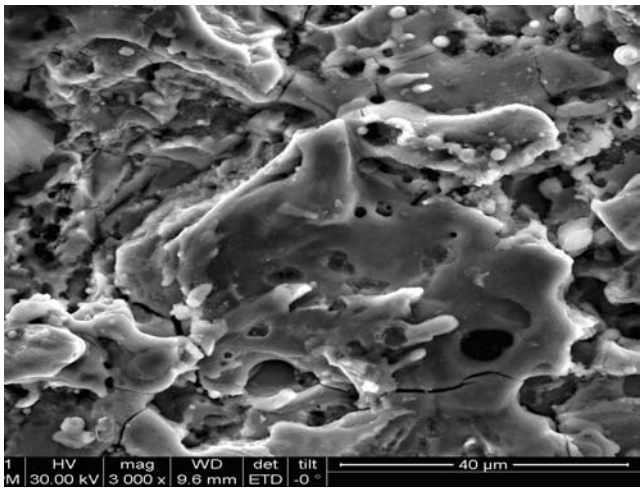

Fig. 10 – SEM micrograph of Ox-Zr2.5Nb3Ta sample.

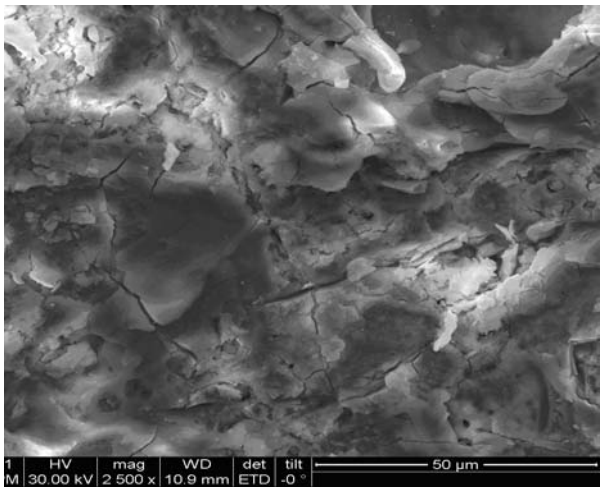

Fig. 11 – SEM micrograph of Ox-Zr10Nb12Ta sample.

In the case of oxidized alloy XRD pattern (Figure 9), there is a number of polymorphic forms of ZrO_2 stable at different temperatures and pressures and it can be especially observed the appearance of two types of zirconium oxides, monoclinic at room temperature and orthorhombic at 573 K,[31-34] which protect the alloy against corrosive attack in the aggressive environment of fetal bovine serum. It seems that the orthorhombic crystallization form corresponds to a black and very stable non-stoichiometric oxide, with excellent anticorrosive properties.

The compared micrographs of the two oxidized samples may be seen in Figures 10 and 11. We can observe an obvious difference in the microstructure and in their surface modification as a result of different amount of alloying elements and the PEO process. It can be noticed that the oxide formed on the surface of highly alloyed sample has a better uniformity and it seems to be more compact than the oxide film formed at the surface of the medium alloyed sample.[34-36]

Vickers hardness is a measure of the hardness of a material, calculated from the size of an impression produced under load by a pyramid-shaped diamond indenter. The indenter employed in the Vickers test is a square-based pyramid whose opposite sides meet at the apex at an angle of 136º. The diamond is pressed into the surface of the material at loads ranging up to approximately 2 kilograms-force, and the size of the impression (usually no more than 0.5 mm) is measured with the aid of a calibrated microscope.

The Vickers number (HV) is calculated using the following formula:

$$HV = 1.854(F/A)$$

with **F** being the applied load (measured in kilograms-force) and **A** the area of the indentation (measured in square millimeters).

This variation of surface Vickers micro-hardness appears due to the formation of a black non-stoichiometric zirconium oxide thin layer during the plasma electrolytic oxidation process. Figures 12 – 15 showed the impressions of the diamond indenter on ZrNbTa and oxidized ZrNbTa alloys. It can be observed that the Vickers microhardness value increases after plasma electrolytic oxidation process with approximately 32% in the case of medium alloyed Zr2.5Nb3Ta (from 448 HV to 592 HV) and with approximately 36% (from 494 HV to 674 HV).

Table 4 show the ICP-MS results for fetal bovine serum electrolyte in which were performed electrochemical measurements for both type of samples. As a result of the examination of the concentration values obtained for different interest elements (Zr, Nb, Ta as raw materials and Co, Cr, Ni, V as ultra trace impurities from raw materials) from the composition of the „used" electrolyte, we can observe a reduction of zirconium concentration passed in solution up to two orders of magnitude, while in the case of niobium and tantalum a reduction with one order of magnitude of the dissolved tantalum concentration value is observed.[36-40] Cytotoxic and allergenic elements like Co, Cr, Ni and V were not observed in the used electrolyte.

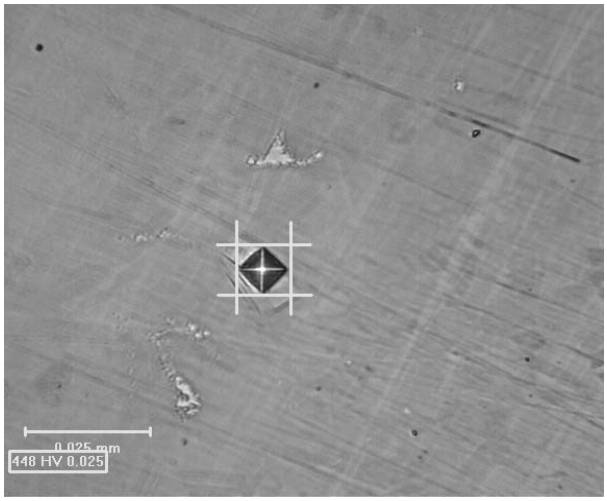

Fig. 12 – Vickers microhardness of Zr2.5Nb3Ta sample.

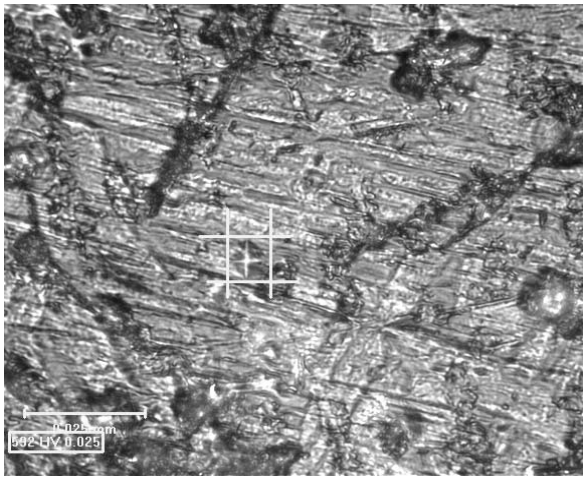

Fig. 13 – Vickers microhardness of Ox-Zr2.5Nb3Ta sample.

Table 4

Ion concentration in electrolyte after polarization measurements

Sample	Concentration, ppm		
	Zr	Nb	Ta
Zr2.5Nb3Ta	33.13	2.28	1.43
Zr10Nb12Ta	28.41	2.70	1.26
Ox-Zr2.5Nb3Ta	0.46	0.19	0.22
Ox-Zr10Nb12Ta	0.33	0.08	0.14

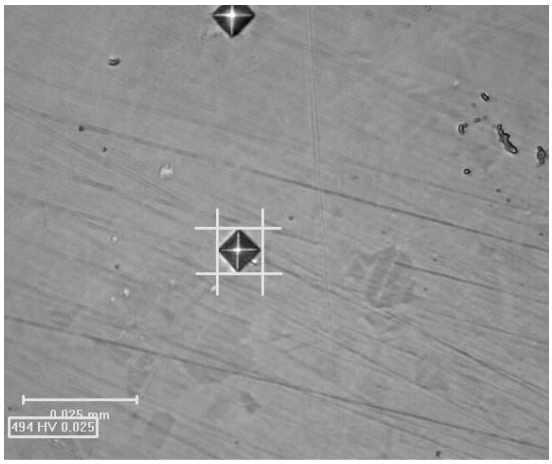

Fig. 14 – Vickers microhardness of Ox-Zr10Nb12Ta sample.

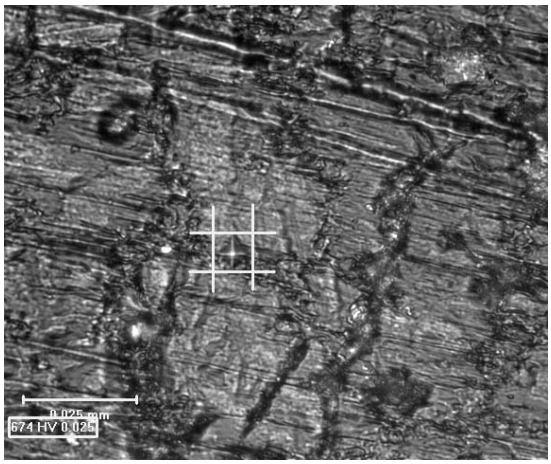

Fig. 15 – Vickers microhardness of Ox-Zr10Nb12Ta sample.

In Figures 16, 17 are presented 3D profiles of the oxidized ZrNbTa surface samples obtained by interferometry measurements with Wyko NT1100 system in VSI (vertical scanning interferometry) mode at the boundary between an area where zirconium oxide layer was removed and the rest of the zirconium oxide area. From diagrams presented in Figures 10a, b, it can be seen that the zirconium oxide layer thickness is about 60 microns.

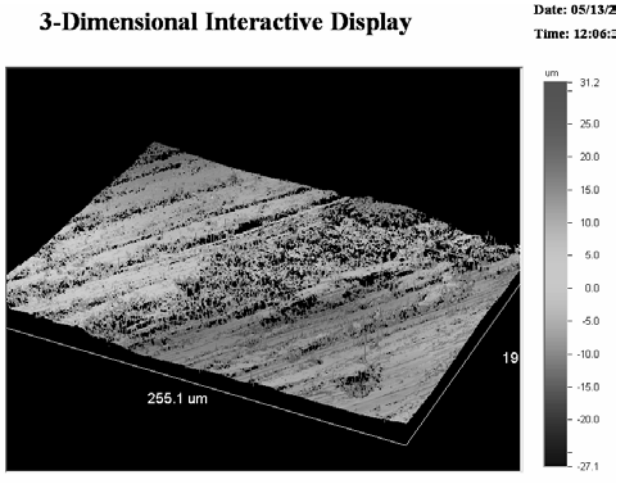

Fig. 16 – 3D profile of Ox-Zr2.5Nb3Ta sample.

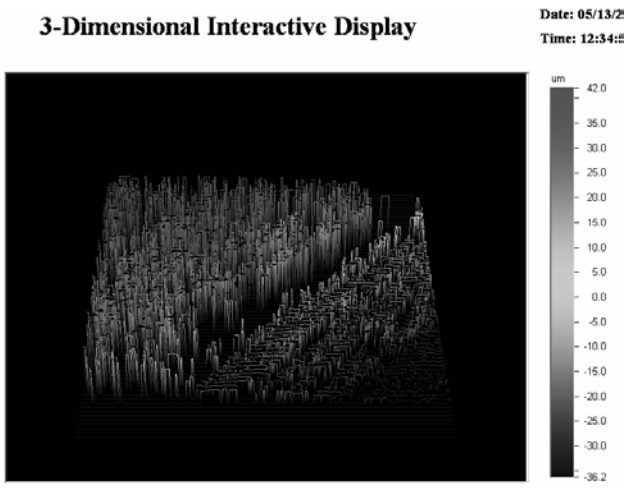

Fig. 17 – 3D profile of Ox-Zr10Nb12Ta sample.

CONCLUSIONS

New biomedical metal-ceramic composites with improved surface properties and higher corrosion resistance were obtained by plasma electrolytic oxidation treatment in alkaline solution.

As a result of the analysis of the polarization curves and kinetic parameters determined through Tafel straight lines extrapolation, a significant improvement of corrosion resistance can be viewed, as a result of the increase of alloying elements amount and the oxidation treatment. Thus, the corrosion current density decreases the polarization resistance of the interface passive film increases, the corrosion rate decreases and the passive potential range increases.

According to EIS measurements, the corrosion resistance increased after the plasma oxidation treating of samples due to the formation of zirconium oxide ceramic layer. In the case of highly alloyed sample the oxide/metal interface is continuous, without pores or voids which might be detrimental to oxide adhesion. The ceramic like zirconia surface layer is highly adherent to the metal alloy and further supported the use of this new alloy as a scratch-resistant counter face for total joint replacement prostheses.

Formation of black non-stoichiometric oxide of about 60 microns thick with protective properties was visually observed and obvious pointed out through X-Ray diffraction analysis, SEM analysis and interferometry measurements. ICP-MS spectra show a significant reduction of ions concentration from fetal bovine serum electrolyte used to alloy samples testing, as a result of heat treatment, which corresponds to the reduction of ion release phenomenon that appears at an orthopedic implant inside the human body during its period of life.

Plasma electrolytic oxidation treatment applied to ZrNbTa alloys improves its corrosion behaviour and reduces the ion release phenomenon. Also, the heat treatment increases alloy biocompatibility, improves the surface mechanical properties and finally, increases the life period of implants made from these materials as well as exploitation security.

Acknowledgements: This study is financially supported by National Grant PNII No. 32-137/2008.

REFERENCES

1. X. Nie, A. Leyland and A. Matthews, *Surf. Coat. Technol*., **2000**, *331*, 133.
2. J. He, Q. Z. Cai, H. H. Luo, L. Yu and B. K. Wei, *J. Alloys Comp*., **2009**, *471*, 395.
3. G. P. WirtZ, S. D. Brown and W. M. Kriven, *Mater. Manuf. Process*., **1991**, *6*, 87.
4. K. Wang, Y. J. Kim, Y. Hayashi, C. G. Lee and B. H. Koo, *J. Cer. Proces. Res*., **2009**, *10*, 562.
5. S. V. Gnedenkov, O. A. Khrisanfova, A. G. Zavidnaya, S. L. Sinebrukhov, P. S. Gordienko, S. Iwatsubo and A. Matsui, *Surf. Coat. Technol*., **2001**, *145*, 146.
6. L. Wang and X. Nie, *Thin Solid Films*, **2006**, *494*, 211.
7. W. B. Xue, X. L. Shi, M. Hua and Y. L. Li, *Appl. Surf. Sci*., **2007**, *253*, 6118.
8. W. Xue, C. Wang, Z. Deng, R. Chen, Y. Lai and T. Zhang, *J. Phys.: Condens. Matter*., **2002,** *14*, 10947.
9. J. A. Curran and T. W. Clyne, *Surf. Coat. Technol*., **2005,** *199*, 168.
10. Y. Wang, T. Lei, B. Jiang and L. Guo, *Appl. Surf. Sci*., **2004**, *233*, 258.
11. D. L. Douglass, "The Metallurgy of Zirconium", Internat. Atomic Energy Agency, Vienna, 1971.

12. A. T. Pichugin, O. H. Luk'yanenko and V. M. Azhazha, *Mater. Sci*., **2000**, *36*, 683.
13. A. D. Montemarano, P. Sau, F. B. Johnson and W. D. James, *J. Am. Acad. Dermatol*., **1997**, *37*, 496.
14. A. A .J. Goldsmith, D. Dowson, G. H. Isaac and J. G. Lancaster, *Proc. Inst. Mech. Eng*., **2000**, *H214*, 39.
15. W. Zhong, J. A. Parkinson, M. Guo and P. J. Sadler, *J. Biol. Inorg. Chem.*, **2002**, *7*, 589.
16. C. Piconi and G. Maccauro, *Biomater.*, **1999**, *20*, 1.
17. J. H. Dubruille, E. Viguier, G. Le Naour, M. T. Dubruille, M. Auriol and Y. Le Charpentier, *Int. J. Oral. Maxillofac. Implants.*, **1999**, *14*, 271.
18. A. Palmieri, F. Pezzetti, G. Brunelli, I. Zollino, L. Lo Muzio, M. Martinelli, L. Scapoli, M. Arlotti, E. Masiero and F. Carinci, *J. Mater. Sci.: Mater. Med.*, **2008**, *19*, 2471.
19. J. Li, Y. Liu, L. Hermansson and R. Soremark, *Clin. Mater*., **1993**, *12*, 197.
20. V. V. Silva, F. S. Lameiras and Z. I. Lobato, *J. Biomed. Mater. Res*., **2002**, *63*, 583.
21. F. Carinci, A. Piattelli, L. Guida, V. Perrotti, G. Laino, A. Oliva, M. Annunziata, A. Palmieri and F. Pezzetti, *Oral Dis*., **2006**, *12*, 329.
22. M. Dedgidi, L. Artese, A. Scarano, V. Perrotti, P. Gehrke and A. Piattelli, *J. Periodontol*., **2006**, *77*, 73.
23. J. Black, "Biological Performance of Materials: Fundamentals of Biocompatibility", Marcel Decker Inc.: New York, 1992.
24. A. Ito, Y. Okazaki, T. Tateishi and Y. Ito, *J. Biomed. Mater. Research*, **2014**, *29*, 893.
25. Y. Chen, X. Nie and D. O. Northwood, *Surface & Coatings Technology*, **2010**, *205*, 1774.
26. V. S. Rudnev, I. V. Malyshev, I. V. Lukiyanchuk and V. G. Kuryavyi, *Protect. Met. Phys. Chem. Surfaces,* **2012**, *48*, 455.
27. W. Xue, Q. Zhu, Q. Jin and M. Hua, *Mater. Chem. Phys.*, **2010**, *120*, 656.
28. M. Montazei, C. Dehfghanianm, M. Shokouhfor, A. Baradaran, *Applied Surface Sci.*, **2011**, *257*, 7268.
29. Y. Cheng, E. Matukina, R. Arrabal, P. Skeldon and G. E.Thomson, *Surface Coatings Technol.,* **2012**, *206*, 3230.
30. M. Sandhyarani, N. Rameshibabu and K. Venkateswarlu, *Surface and Coatings Technol.*, **2014**, *238*, 58.
31. E. H. Kisi, C. J. Howard, R. J. Hill, *J. Am. Ceram. Soc.*, **1989**, *72*, 1757.
32. H. McMurdie, M. Morris, E. Evans, B. Paretzkin, W. Wong-Ng and C. Hubbard, *Powder Diffraction*, **1986**, *1*, 275.
33. Y.-L. Cheng and W. Fan, Transact. *Nanofer. Met. Soc. China*, **2014**, *22*, 1638.
34. S. Aurdu and M. Usta, *Ceramic Int.*, **2014**, *20*, 3627.
35. M. Sandhyaroni, N. Roweshbabu, K. Venkatesuarlu, D. Sreekanth and Ch. Subrahmanyam, *J. Alloys Compounds*, **2013**, *553*, 324.
36. H.-Z. Li and J. Xu, *J. Mechanical behavior Biomed. Mater.*, **2014**, *32*, 166.
37. N. Sakaguchi, M. Niinomi, T. Akahori, J. Takeda and H. Toda, *J. Japan Instit. Met.*, **2004**, *68*, 1076.
38. X.-M. Ma, W. Sun and Y.-J. Yang, *Chinese J. Nonferr. Met.*, **2010**, *20*, 1195.
39. Y. Cheng, J. Cao, Z. Peng, Q. Wang, E. Matykina, P. Skeldon and G. E. Thompson, *Electrochim. Acta*, **2014**, *116*, 453.
40. Y. Cheng, F. Wu, J. Doug, X. Wu, P. Skeldon and G. E.Thomson, *Electrochimica Acta*, **2012**, *85*, 25.